Lift Enhancement by an Externally Trapped Vortex

Vernon J. Rossow*
NASA Ames Research Center, Moffett Field, Calif.

A theoretical study is made of the performance capabilities of a lift concept that utilizes a spanwise vortex over the upper surface of the wing. The vortex is generated by a vertical flap near the leading edge of the wing and maintained by suction through orifices in endplates at the wingtip. The analysis approximates the three-dimensional flowfield with a two-dimensional configuration that is mapped by conformal transformation into the flow about a circle. Theoretical solutions for a range of flap and orifice configurations predict that section lift coefficients up to around 10 can be achieved. It is concluded that such a lift concept is applicable to STOL aircraft if the vortex can be adequately stabilized and if the endplate suction can be generated efficiently.

Nomenclature

b = wing span
c = chord
C_D = drag coefficient
C_L = lift coefficient
L_{fl} = flap-length parameter
$\dot{m}_x$ = source strength at external equilibrium point, negative values denote sink
r = radius
R = r/r_c
u,v = velocity components in x and y directions
U_∞ = freestream velocity, aligned with x axis
x,y = coordinate axes
x_{fl} = chordwise distance from airfoil nose to attachment point of flap base
Z = $x+iy$, complex variable (see Fig. 3)
α = airfoil angle of attack from zero lift
β_{rk} = flap curvature parameter used in conformal mapping (see Fig. 3)
Γ_a = bound circulation on or inside airfoil
Γ_x = circulation in external vortex
θ = meridian angle in various mapping planes (see Fig. 3)
θ_{fl} = flap angle parameter in conformal mapping that governs chordwise flap attachment point on airfoil, x_{fl}
θ_{xoc} = meridian angle in original circle plane to external vortex
Φ = complex potential

Subscripts

A = airfoil plane
AF = final airfoil plane
c = circle plane
cr = rotated circle plane (Fig. 3)
oc = original circle plane
x = external vortex or equilibrium point location

Introduction

THE development of vertical and short takeoff and landing (V/STOL) aircraft is dependent on methods for achieving high lift coefficients on the wings of these vehicles. Past research (e.g., Refs. 1-8) has considered a wide variety of passive and active lift-generating mechanisms, such as multielement flap systems, internally and externally blown flaps, etc., each with certain advantages and disadvantages. The present investigation considers the performance capabilities of a lift concept that is based on generating and maintaining a spanwise vortex over the upper surface of the wing. This concept is an extension of the lift enhancement that occurs when an organized vortex occupies the separated flow region over highly swept wings at large angles of attack (e.g., Refs. 9 and 10). The vortex occurs near and parallel to the leading edge of the wing, shielding it from the oncoming airstream. The spanwise pressure gradient due to sweep evacuates the vortex core, thereby organizing the angular momentum in the separation zone into a conically shaped vortex. As the sweep and angle of attack of the wing are reduced, the vortex position becomes unstable. Some mechanism must then be added to the wing to evacuate the core region in order to organize the angular momentum into a vortex and to hold (or trap) the vortex in place.

Several techniques have been used in the past to generate and stabilize vortices on top of the wing or inside a cavity within the wing. One of the less complicated schemes is to direct a jet of air spanwise toward the wingtip along the surface of the wing[11-15] to enhance the lift from the external vortex over swept wings. Other ways that have been studied are to replace the vortex with a rotating cylinder[16-21] and to generate the vortex either 1) on top of the wing or 2) inside a cavity located within the wing.[22-26] All of these techniques produce (in the flowfield over the wing) a locally rotating motion that simulates a thickening of the wing. The low pressure in the vicinity of the rotating flow (or vortex) produces the lift enhancement of the wing.

The flowfield under consideration in this investigation is shown schematically in Fig. 1. The external vortex lies downstream of the flap near the leading edge and spanwise along the upper surface of the wing between two endplates that contain orifices for removing air from the vortex core. One of the endplates could be envisioned as part of the aircraft fuselage, and the other, as part of the wingtip that rotates to the vertical. The wingtip segment and the leading-edge flap would be deployed for vortex generation during landing and takeoff only. The purpose of the flap is to separate the flow along the leading edge of the wing, thereby introducing angular momentum into the air, which is then organized into a vortex by suction through the orifices in the endplates. The resulting spanwise vortex that occupies the separation zone needs the flap, not only for its generation, but also for protection and stability against the oncoming airstream. The endplates serve as 1) barriers that protect the low-pressure region over the wing, 2) attachment points for the

Presented as Paper 77-672 at the AIAA 10th Fluid and Plasma Dynamics Conference, Albuquerque, N. Mex., June 27-29, 1977; submitted July 22, 1977; revision received May 23, 1978.

Index category: Aerodynamics.

*Staff Scientist. Associate Fellow AIAA.

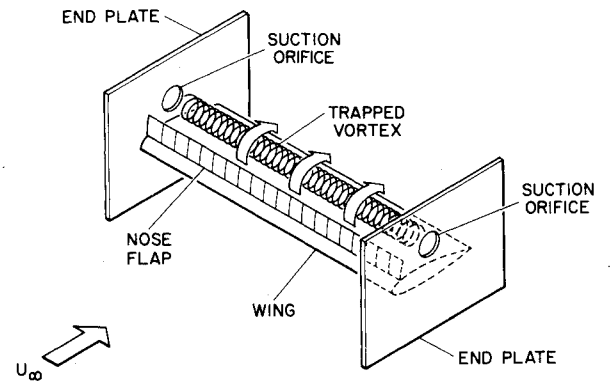

Fig. 1 Schematic diagram of trapped vortex showing wing, nose flap, and endplates with suction orifices.

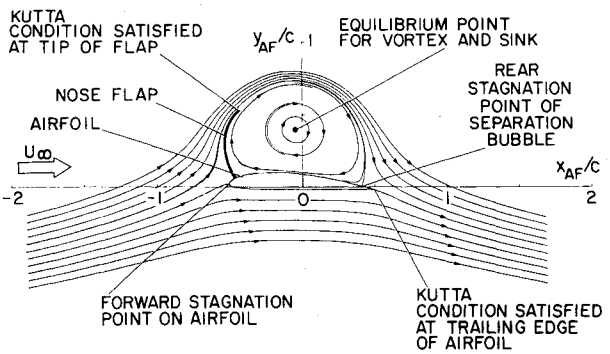

Fig. 2 Two-dimensional flowfield model used to determine incompressible values of sink and vortex strengths required to satisfy boundary conditions on airfoil and flap: $C_L = 6.06$, $C_D = 0.161$, $\Gamma_x/cU_\infty = -5.39$, $\Gamma_a/cU_\infty = 2.39$, $\dot{m}_x/cU_\infty = -0.047$, $\alpha = 0.1$, $\beta_{rk} = -0.75$, flap chord = 0.4c; flap base attached to airfoil at 0.05 c ($\theta_{fl} = 2.725$).

vortex, and 3) supports for the suction orifices that locate and hold the vortex center at a given location.

This paper first describes the flow model and theoretical method used in the analysis of the externally trapped vortex/airfoil combination. The characteristics of the flowfield are then studied for a range of the governing parameters. In the study are found compatibility conditions that relate the lift on the system to the flap size and shape to the airfoil angle of attack and to the location and strengths of the sink and vortex. These results are followed by an approximate analysis of the stability of the vortex and sink location.

Analysis of Flowfield

Description of Flow Model and Boundary Conditions

The present analysis approximates the three-dimensional flowfield (Fig. 1) with the two-dimensional flow model shown in Fig. 2. It assumes spanwise velocities to be negligible (except near the center of the external vortex, where a sink is placed to approximate removal of air through the orifices in the endplates). The analysis also assumes that the sink and vortex centers are at the same location and that compressibility, viscosity, turbulence, and flow separation are negligible, which thereby allows the use of incompressible, potential-flow theory. The analysis is then greatly simplified by use of conformal transformations[27] which map the flow about the airfoil and flap from the flow about a circle (Figs. 3 and 4). Boundary conditions in the airfoil plane require that: 1) the flow depart smoothly from the free end of the leading-edge flap and from the airfoil trailing edge (i.e., the Kutta condition must be satisfied there); 2) the vortex/sink combination be located at an equilibrium point in the flowfield, that is, a point where the velocity produced by all other influences is zero; 3) since the separation bubble containing the

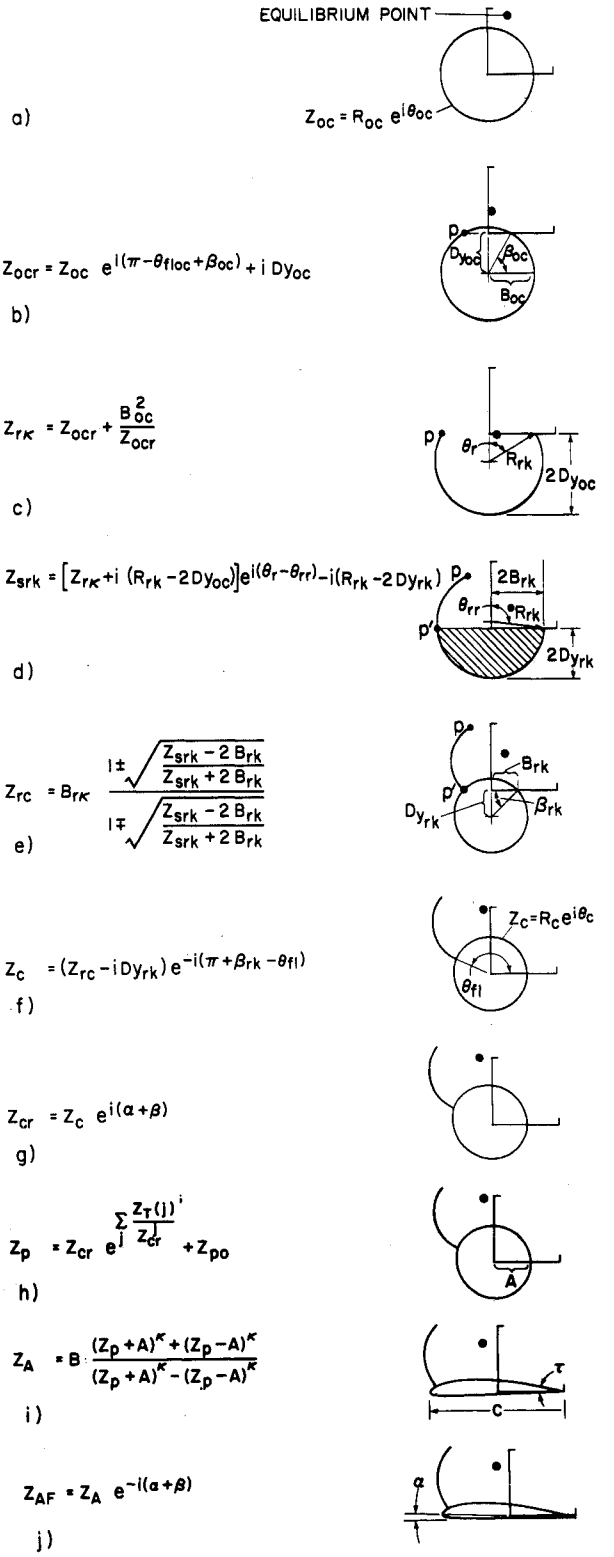

Fig. 3 Steps in mapping sequence from original circle (Z_{oc}) plane to final flapped-airfoil (Z_{AF}) plane, shown in Fig. 8a: $\alpha = 0.1$, $\theta_{fl} = 2.725$, $\beta_{rk} = -0.75$, $L_{fl} = 0.40$, $r_{xoc}/c = 0.473$, $\theta_{xoc} = 1.239$, $\Gamma_x/cU_\infty = -4.864$, $\Gamma_a/cU_\infty = +2.364$, $\dot{m}_x/cU_\infty = -0.0488$, $C_L = 5.0$.

vortex must be closed on the upper surface of the airfoil, its rear stagnation point must occur ahead of the trailing edge; and 4) a forward stagnation point occur on the airfoil nose or on the front face of the leading-edge flap.

Another aspect of the flow to be noted is that the streamline which impacts the forward stagnation point also wets the lower surface of the airfoil and the front face of the flap. It

does not, however, touch the upper surface of the airfoil nor the rear face of the flap, but spirals into the sink/vortex pair at the equilibrium point. Furthermore, the streamline that impacts at the stagnation point at the rear of the vortex bubble wets the aft portion of the airfoil and divides the airstream that enters the sink from the one that passes above the airfoil/vortex combination. The other branch of this streamline moves forward to wet the forward part of the airfoil under the vortex bubble and the rear face of the flap, and then it spirals into the sink.

Conformal Transformation Used to Analyze Flowfield

The conformal mapping process makes it possible to find the parameters (the location of the equilibrium point and the strengths of the sink and vortex required for a given lift) which insures that the foregoing boundary conditions are satisfied. A solution for the flowfield is provided by a mapping sequence that transforms the potential flow about a circle into a flow about an airfoil with an attached leading-edge flap or spoiler in the presence of an external vortex/sink combination. This indirect method requires that the shape of the flap be iterated by varying parameters in the mapping equations until the resulting flap shape approximates the desired one. The transformation used is an adaptation of that in Ref. 27, wherein the flow exterior to the airfoil now includes the contribution of one or more singularities (source, sink, or vortex) located at an equilibrium point in the flowfield. The essential features of this method are presented here because the conformal transformation is a central part of the study reported herein.

The transformation which generates a flap on an airfoil is illustrated in Fig. 3 as ten steps from a circle to the flapped airfoil. (The Clark Y airfoil[28] was used in all the illustrations because the coefficients $Z_T(j)$ were available from another investigation.) The mapping equations are shown beside each figure. The amounts of rotation and translation given to the circle and arc during the various steps govern the length of the flap, its curvature, and its location on the airfoil. A flap-curvature parameter β_{rk} and a flap-length parameter L_{fl} are used to govern the mapping of the original circle into a circular slit (Z_{rk} plane), to rotate and shift the slit (Z_{srk} plane), and to map the shortened arc into a circle with a flap (Z_c plane). The mapping functions used to obtain this figure must be such that the circular portion is an exact circle of radius R_c (Fig. 3f) so that it can be transformed into an airfoil by Theodorsen's method.[29] Therefore, once the angle that locates the flap in the circle plane (i.e., θ_{fl} in Fig. 3f) and the parameters β_{rk} and L_{fl} are chosen, the other quantities in the mapping sequence are determined by the following equations:

$$Dy_{rk} = R_c \sin\beta_{rk} \qquad B_{rk} = R_c \cos\beta_{rk} \tag{1a}$$

$$R_{rk} = R_c / \sin\beta_{rk} \qquad \theta_{rr} = 2\beta_{rk} \tag{1b}$$

$$\theta_r = \theta_{rr}(1 + L_{fl}) \qquad B_{oc} = (R_{rk} \sin\theta_r)/2 \tag{1c}$$

$$Dy_{oc} = R_{rk}(1 - \cos\theta_r)/2 \tag{1d}$$

$$\beta_{oc} = \tan^{-1}(Dy_{oc}/B_{oc}) = \theta_r/2 \tag{1e}$$

$$R_{oc} = B_{oc}/\cos\beta_{oc} \tag{1f}$$

The amount of rotation in the various planes must be such that the freestream returns to its original direction in both the circle or Z_c and in the final or Z_{AF} planes. The various angles are then related by

$$\theta_{floc} = \theta_{fl} - \beta_{rk} + \beta_{oc} + \theta_r - \theta_{rr} \tag{2}$$

where θ_{floc} locates the tip of the flap in the original circle plane as shown in Fig. 3. The flap-curvature parameter is limited in that it cannot exceed 90 deg; that is, $-\pi/2 \le \beta_{rk} \le +\pi/2$. Likewise, the angular segment of the circular arc slit in Fig. 3c cannot exceed 2π, so

$$|\theta_r| \le \pi$$

The flap-length parameter is therefore limited by

$$0 \le L_{fl} \le [(\pi/2|\beta_{rk}|) - 1] \tag{3}$$

The quantities used in the transformation of the flapped circle (Fig. 3f) into the flapped Clark Y airfoil at angle of attack (Fig. 3j) are: the angle of attack of the airfoil from zero lift α; the angle-of-zero lift from the geometric chord line β; and the Theodorsen coefficients $Z_T(j)$ and the shift of the potato curve, as listed below:

$$\beta = -0.05906$$

$$Z_T(1) = (-0.07671 + i1.18942)\,10^{-3}$$

$$Z_T(2) = (+1.22322 - i1.25433)\,10^{-3}$$

$$Z_T(3) = (-0.04961 + i0.07613)\,10^{-3}$$

$$Z_T(4) = (+0.01615 - i0.05246)\,10^{-4}$$

$$Z_T(5) = (+0.6174 + i0.1708)\,10^{-6}$$

$$Z_T(6) = (-0.5788 + i0.6464)\,10^{-7}$$

$$Z_{po} = -0.019332 + i0.020158 \tag{4}$$

The parameters A and κ are related to the trailing-edge angle τ, the nose radius R_n, and the chord of the airfoil by

$$\kappa = 2 - \tau/\pi = 1.91487$$

$$A = (c - R_n/2)/\kappa = 0.26088 \tag{5}$$

It is convenient to relate the various lengths to the chord c of the airfoil so that they are dimensionless.

Once the flapped circle has been generated, the flap portion of the figure is carried along without special attention, while the circle portion is being mapped into the desired airfoil at angle of attack. During this process, the flap or segment of the arc originally dedicated to the flap is carried along as a vanishingly small slit. Its shape is modified from circular in the Z_{rk} and Z_{srk} planes to a nondescript shape in the final airfoil plane. This shape can differ considerably from the original one in curvature and length, making it necessary to iterate on the various flap parameters to arrive at a shape that approximates the desired one.

The only step in the mapping sequence where special attention must be given to the signs or roots of the functions is the one shown in Fig. 3d where the square root is taken. A continuous mapping is obtained if the lower sign on the square root is used when Z_{srk}, the point being transformed, lies within the cross-hatched area between the horizontal or real axis and the arc as shown in Fig. 3d. The upper sign is used when the point is elsewhere in the flowfield. This assures the development of both the upper and lower segments of the circle from the circular arc slit. In the calculations, it is convenient to let the original circle be slightly larger than the theoretical value (i.e., increase R_{oc} by 0.0001) to make it possible for the computer to discern whether a point is on the upper or lower portion of the circular arc slit.

The velocity components are found in each of the planes from

$$d\Phi/dZ_{AF} = (d\Phi/dZ_{oc})(dZ_{oc}/dZ_{AF}) = u - iv \tag{6}$$

The streamline pattern, pressures, etc., can then be calculated in closed form for the airfoil with its attached flap after the derivatives dZ_{oc}/dZ_{AF} are found from the mapping functions.

Equation (6) cannot be used to find the conditions which make the velocity vanish at the location of the sink and vortex because the velocity given by Eq. (6) is singular there. The usual limiting process used to find the velocity components at the center of a vortex or sink combination is applied here at the external vortex location. The strengths of the singularities can then be adjusted so that they are stationary in the presence of the flapped airfoil. The velocity at the location of the singularities in the original circle plane, Z_{oc}, is found as

$$(u_{oc}-iv_{oc})\,|_{Z_{oc}-Z_{xoc}} = \frac{d}{dZ_{oc}}\left\{\lim_{Z_{oc}\to Z_{xoc}}\left[\Phi(Z_{oc}) - \begin{pmatrix}\text{complex potential due}\\ \text{to external source and}\\ \text{vortex}\end{pmatrix}\right]\right\}$$

$$= \frac{d}{dZ_{oc}}\left\{\lim_{Z_{oc}\to Z_{xoc}}\left[\Phi(Z_{oc}) + \frac{i\Gamma_x+\dot{m}_x}{2\pi}\ln(Z_{oc}-Z_{xoc})\right]\right\} \quad (7)$$

where the limiting process is straightforward. In the final or flapped airfoil plane, the velocity components at the equilibrium point are given by

$$(u_{AF}-iv_{AF})\,|_{Z_{AF}-Z_{x_{AF}}} = \frac{d}{dZ_{AF}}\left\{\lim_{Z_{AF}\to Z_{x_{AF}}}\left[\Phi(Z_{AF}) + \frac{i\Gamma_x+\dot{m}_x}{2\pi}\ln(Z_{AF}-Z_{x_{AF}})\right]\right\} \quad (8)$$

Since these functions are analytic and the transformations conformal, the following equalities hold:

$$\Phi(Z_{AF})=\Phi(Z_{oc}) \qquad \Gamma_x|_{Z_{AF}}=\Gamma_x|_{Z_{oc}} \qquad \dot{m}_x|_{Z_{AF}}=\dot{m}_x|_{Z_{oc}}$$

When the contributions of the singularities in the circle plane are added and subtracted, the complex velocity function in the flapped airfoil plane can be written as

$$(u_{AF}-iv_{AF})\,|_{Z_{AF}-Z_{x_{AF}}} = \frac{d}{dZ_{AF}}\left\{\lim_{Z_{AF}\to Z_{x_{AF}}}\left[\Phi(Z_{oc}) + \frac{i\Gamma_x+\dot{m}_x}{2\pi}\ln(Z_{oc}-Z_{xoc}) - \frac{i\Gamma_x+\dot{m}_x}{2\pi}\ln\frac{Z_{oc}-Z_{xoc}}{Z_{AF}-Z_{x_{AF}}}\right]\right\} \quad (9)$$

In order to take the limiting process, it is necessary to expand the transformation variable in a power-series expansion as

$$Z_{oc} = Z_{xoc} + (Z_{AF}-Z_{x_{AF}})\frac{dZ_{oc}}{dZ_{AF}}\Big|_{Z_{x_{AF}}} + \frac{(Z_{AF}-Z_{x_{AF}})^2}{2}\frac{d^2Z_{oc}}{dZ_{AF}^2}\Big|_{Z_{x_{AF}}} + \ldots \quad (10)$$

When Eq. (10) is substituted into Eq. (9), and the limit taken, the complex velocity function in the flapped airfoil plane at the equilibrium point is given by

$$(u_{AF}-iv_{AF})\,|_{Z_{x_{AF}}} = (u_{oc}-iv_{oc})\frac{dZ_{oc}}{dZ_{AF}}\Big|_{Z_{xoc}} - \frac{i\Gamma_x+\dot{m}_x}{4\pi}\left(\frac{d^2Z_{oc}}{dZ_{AF}^2}\Big|_{Z_{x_{AF}}}\Big/\frac{dZ_{oc}}{dZ_{AF}}\Big|_{Z_{x_{AF}}}\right)=0 \quad (11)$$

When the derivatives of the various mapping functions are found from the functions listed in Fig. 3, the location and strengths of the vortex and sink can be found so that they are stationary in the flapped airfoil plane. The boundary conditions on the airfoil and flap, and the Kutta condition on the trailing edges of the flap and airfoil provide the needed restraints to make all of the unknowns determined. Since it was impossible to separate the foregoing equations for an explicit relationship for the location and strengths of the singularities, the solution was found by an iterative process. After the location of the equilibrium point and the strengths

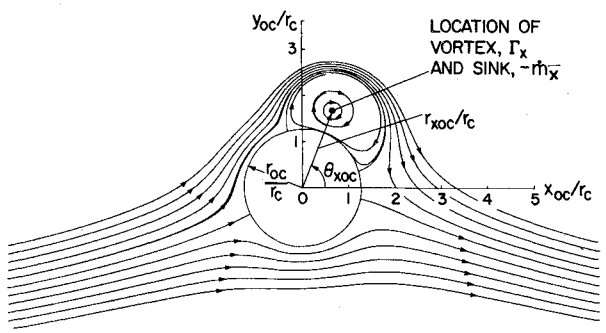

Fig. 4 Flowfield in original circle plane before mapping by conformal transformations into solution for flapped-airfoil plane shown in Fig. 2.

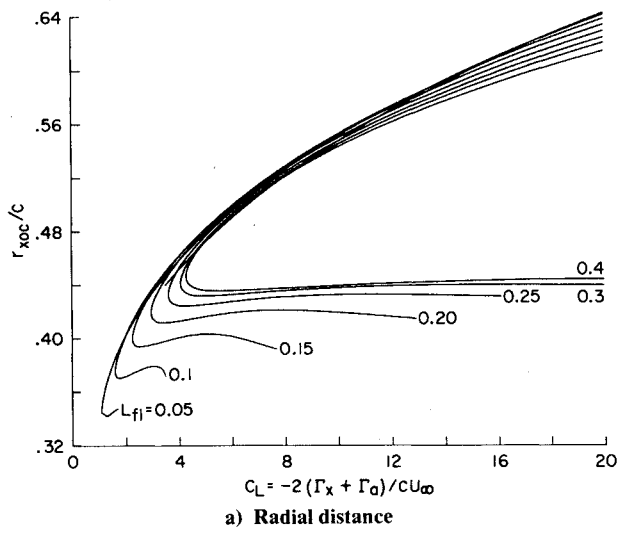

a) Radial distance

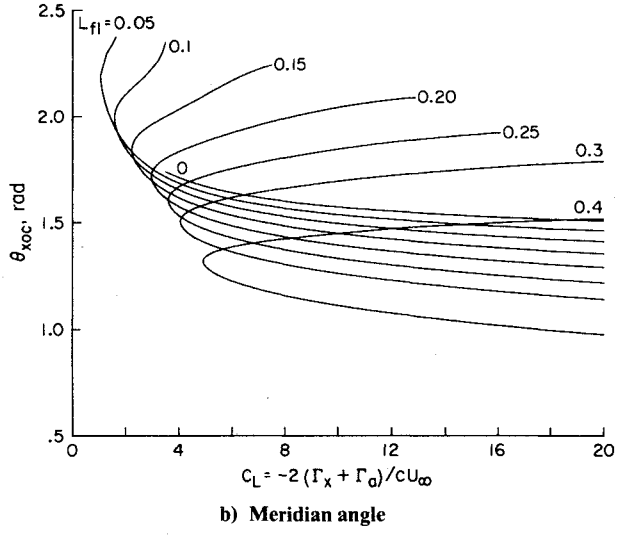

b) Meridian angle

Fig. 5 Variation of location of equilibrium point as a function of lift coefficient for various flap-length parameters, L_{fl}: $\beta_{rk}=-0.75$, $\theta_{fl}=2.725$ ($x_{fl}=0.05c$), $\alpha=0.10$.

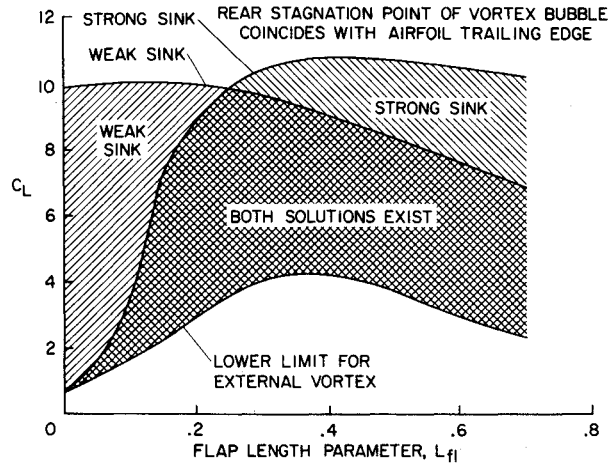

Fig. 6 Range of lift coefficients possible for $\alpha = 0.1$, $\beta = -0.75$, $x_{fl}/c = 0.05$ ($\theta_{fl} = 2.725$).

of the vortex and sink are known, the potential, stream function, and velocity components are available in closed form from the foregoing equations. The flowfield in the original circle plane (Fig. 4) is then known in closed form and can be mapped into the flow about a flapped airfoil (Fig. 2).

Variation of Lift with Flowfield Parameters

In this section, examples are presented to illustrate how much lift can be achieved with an externally trapped vortex and how the lift changes with the various flowfield parameters. In the examples to follow, the flap curvature parameter, β_{rk}, was chosen to provide a nearly circular shape to fit the contour of the vortex bubble. Other nearby values should yield comparable results.

The first step in the study of the lifting characteristics of the externally trapped vortex concept is to find (using the equations developed in previous sections) the location of the equilibrium point and the strengths of the sink and vortex for a range of conditions. Variations of radius r_{xoc} and meridional angle θ_{xoc} to the external vortex or equilibrium point location in the original circle (or Z_{oc}) plane, found from Eq. (11), are presented in Fig. 5 for a range of lift coefficients C_L and flap sizes L_{fl}. Note that, for a given lift, the equations yield two possible solutions for the locations of the equilibrium points and for the corresponding strengths of the vortex and sink. The two solutions differ mostly in the strength of the sink and the drag of the system, since the vortex strengths are closely related to the lift which is the same for the two solutions. As noted in Fig. 5, both solutions indicate that large-section lift coefficients are possible for a variety of flap sizes. It is necessary, however, to check these preliminary results to see whether the Kutta condition is satisfied in every case at the flap and airfoil trailing edges. When the points on the airfoil (or on the cylinder in the original circle plane) at which the flow stagnates or separates from the surface are located, an upper limit is found for the lift on each configuration. Above this limit occurs unrealistic supercirculation, wherein some of the streamlines may go entirely around the system at the larger values of C_L. These restraints produce boundaries or domains for which realistic solutions exist for the trapped vortex flowfield. The example, shown in Fig. 6, illustrates maximum and minimum lift coefficients that are possible for a range of flap sizes when the nose flap attachment point is 5% aft of the leading edge of the airfoil. As indicated in Fig. 5, the same lower limit on lift exists for the high (strong sink) and low (weak sink) drag solutions. Although, as shown in Fig. 6, a different upper boundary on lift occurs for the two solutions, both are capable of yielding lift coefficients in the vicinity of 10 for a range of flap sizes when the flap is attached to the airfoil at

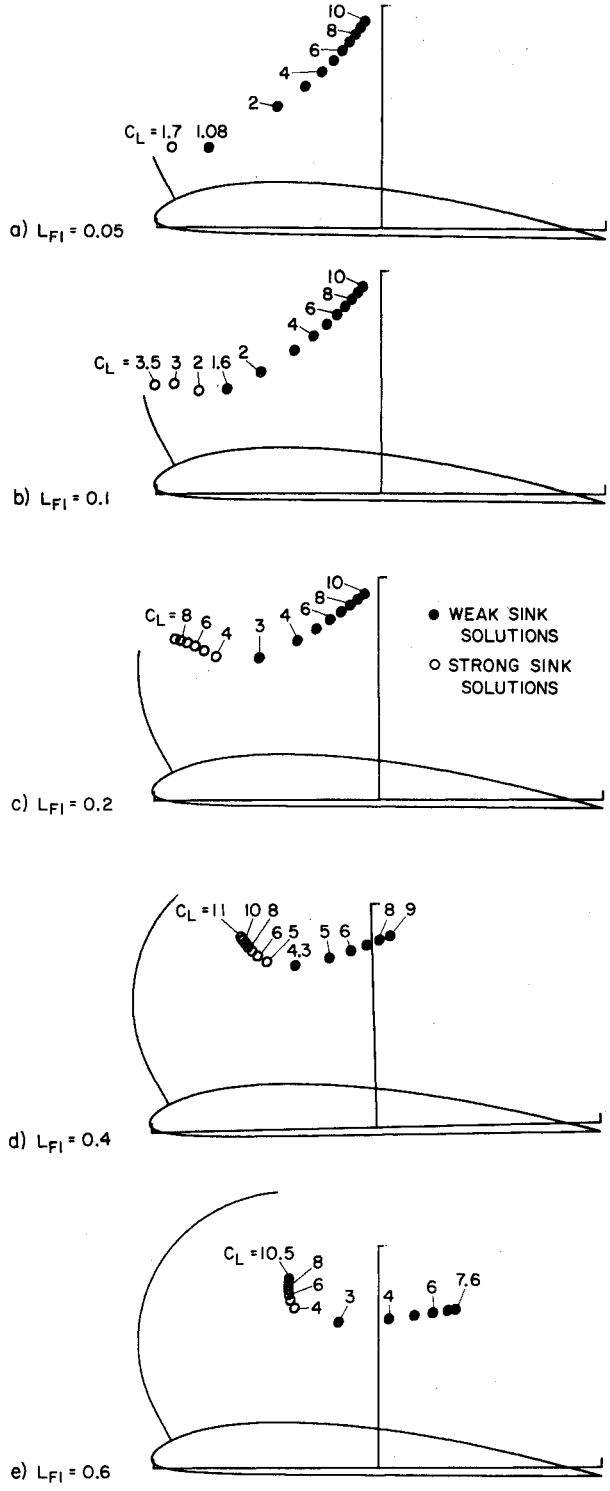

Fig. 7 Locations of equilibrium points for various integer and limiting values of C_L and various values of flap-length parameter, L_{fl}: $\alpha = 0.10$, $\beta_{rk} = -0.75$, $x_{fl}/c = 0.05$ ($\theta_{fl} = 2.725$).

the 5% chord position. Other flap curvature parameters, flap attachment points, etc., would yield a different range of conditions.

From the results in Figs. 5 and 6, a series of locations for the equilibrium point relative to the airfoil and flap are shown in Fig. 7 for several flap lengths. These results illustrate how the lift on the system and the flap length affect the location of the center of the endplate orifice. Hence, not only does the mass flow through the orifice, but its location must also change with lift, angle of attack, and flap shape and position. In practice then, the endplate orifice must either be moveable

or large enough to accommodate the required position changes in the center of the vortex and sink for the anticipated range of lift coefficients and flap changes. In other words, the variations in vortex and sink strength with the various parameters provide a means for controlling the lift and drag of the system through a change in the location, suction, and, possibly, the size of the endplate and its orifice.

The streamline patterns for several lift coefficients in both the low (Fig. 8) and the high (Fig. 9) sink-strength cases illustrate the nearly circular nature of the airfoil/vortex configuration. In each of these examples, the streamlines fulfill the boundary conditions specified in a foregoing section. That is, the flow separates at the tip or upper end of the nose flap to form a vortex bubble over the airfoil upper surface. This streamline first impacts the forward stagnation point and then divides to wet the front face of the flap and the lower surface of the airfoil. It does not, however, touch the upper surface of the airfoil nor the rear face of the flap, but spirals into the sink/vortex combination at the equilibrium point. Furthermore, the streamline that impacts at the stagnation point at the rear of the vortex bubble wets the aft portion of the airfoil and divides the airstream which enters the sink from that which passes above the airfoil/vortex combination. The other branch of this streamline moves forward to wet the forward part of the airfoil under the vortex bubble and the rear face of the flap, and then it spirals into the sink. As expected, the beginning space between the two stagnation streamlines is much larger for the strong-sink (Fig. 9) than for the weak-sink solutions (Fig. 8) because of the higher mass flow into the equilibrium point location.

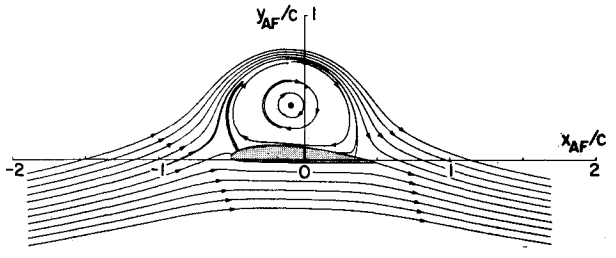

a) $C_L = 5.08$, $C_D = 0.174$, $\Gamma_x/cU_\infty = -4.864$, $\Gamma_a/cU_\infty = 2.364$, $\dot{m}_x/cU_\infty = -0.0488$.

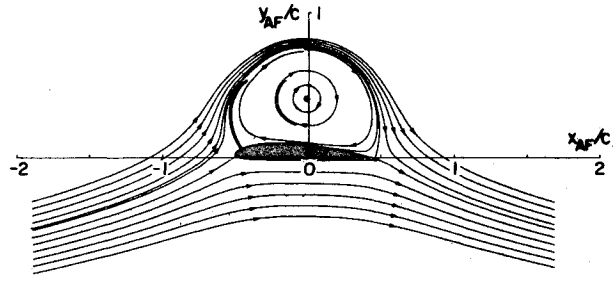

b) $C_L = 7.05$, $C_D = 0.177$, $\Gamma_x/cU_\infty = -5.905$, $\Gamma_a/cU_\infty = 2.405$, $\dot{m}_x/cU_\infty = -0.0563$.

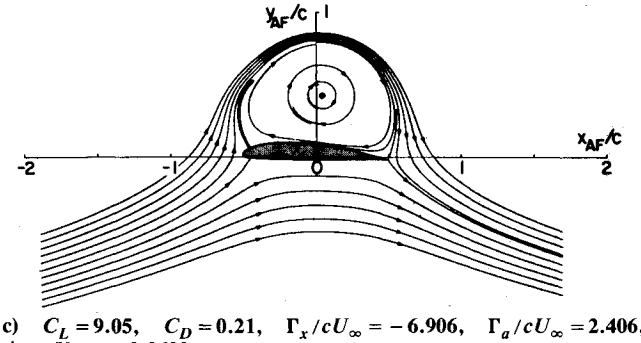

c) $C_L = 9.05$, $C_D = 0.21$, $\Gamma_x/cU_\infty = -6.906$, $\Gamma_a/cU_\infty = 2.406$, $\dot{m}_x/cU_\infty = -0.0692$.

Fig. 8 Streamlines and flow parameters for three lift values on airfoil: $x_{fl}/c = 0.05$ ($\theta_{fl} = 2.725$), $\beta_{rk} = -0.75$, $\alpha = 0.10$, $L_{fl} = 0.4$.

As other examples (Fig. 10), the streamlines are presented for the cases wherein the flap is attached at the 10%, 25%, and 50% chord positions on the airfoil to illustrate how the size of the vortex bubble is reduced as the flap-attachment point moves aft. The corresponding dependence of the maximum lift achievable as a function of the chordwise location of the flap attachment point is presented in Fig. 11. The reduced lift for the aft flap locations is caused by the restriction in the area over the upper surface of the airfoil on which the external vortex can augment the lift. That is, a trailing-edge flap provides no opportunity for lift enhancement and a leading-edge flap provides the largest vortex cavity and, therefore, the maximum lift enhancement possible for a given flap size and flap shape.

When the computations similar to those presented in Figs. 5-9 are made for airfoil angles of attack equal to 0.15 and 0.20 rad, the increment in maximum lift (Fig. 12) due to angle of attack is about the same as for an airfoil without a flap or externally trapped vortex. Since the shape of the streamline surface of the airfoil/vortex bubble is approximately circular at maximum lift, only a small change in $C_{L\,max}$ would be expected.

Stability of Trapped Vortex

The foregoing analysis establishes the equilibrium position and strengths of the vortex/sink pair, but does not address the problem of stability nor flap size. For these reasons, a time-dependent calculation was made of the motion of the singularities when their position is displaced a given amount (e.g., to the locations marked by x's in Fig. 13). The theory assumed that the singularity strengths remained constant during the excursion, even though the Kutta condition at the flap and airfoil trailing edges are then usually not satisfied. It was hoped that the singularities would return to the equilibrium position for flap sizes larger than a certain amount. These configurations would then be considered stable and a minimum flap size would be established. Unfortunately, the results of the calculations for a number of cases indicated that the vortex/sink pair would return to its equilibrium location only from a limited region of starting points (e.g., point A in Fig. 13). It was concluded, therefore, that the flowfield stability was delicate and that a more complete theory for the flowfield is needed to establish flap size requirements.

Other Flowfield Considerations

When the externally trapped vortex concept is applied to flight hardware, a variety of other flowfield parameters will have an influence on the design. For example, wing design features such as sweep, taper, etc. will require that the spanwise structure of the vortex be adapted to the structure available. Also, viscous effects and three-dimensional effects,

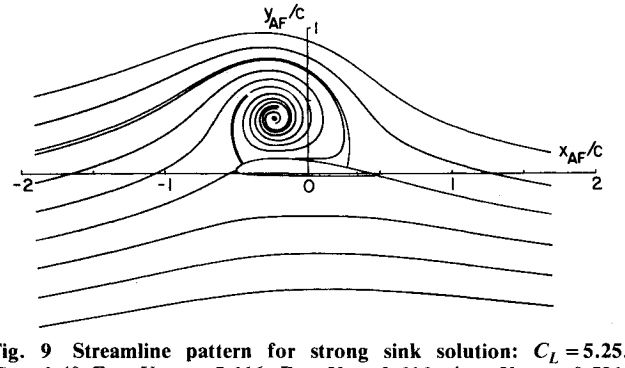

Fig. 9 Streamline pattern for strong sink solution: $C_L = 5.25$, $C_D = 1.40$, $\Gamma_x/cU_\infty = -5.116$, $\Gamma_a/cU_\infty = 2.616$, $\dot{m}_x/cU_\infty = -0.591$, $\alpha = 0.10$, $L_{fl} = 0.40$, $\beta_{rk} = -0.75$, $x_{fl}/c = 0.05$ ($\theta_{fl} = 2.725$).

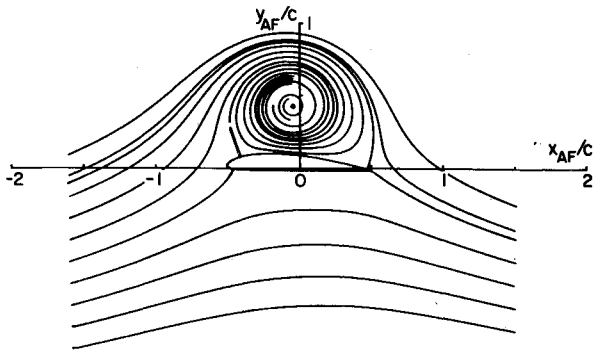

a) $x_{fl}/c = 0.10$ ($\theta_{fl} = 2.509$), $\beta_{rk} = -0.50$, $L_{fl} = 0.1$, $\Gamma_x/cU_\infty = -6.679$, $\Gamma_a/cU_\infty = 2.679$, $\dot{m}_x/cU_\infty = -0.451$, $C_L = 8.0$, $C_D = 0.93$.

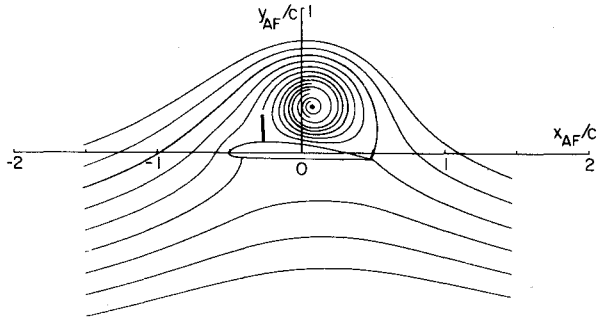

b) $x_{fl}/c = 0.25$ ($\theta_{fl} = 2.062$), $\beta_{rk} = -0.50$, $L_{fl} = 0.05$, $\Gamma_x/cU_\infty = -5.442$, $\Gamma_a/cU_\infty = 1.942$, $\dot{m}_x/cU_\infty = -0.385$, $C_L = 7.0$, $C_D = 0.81$.

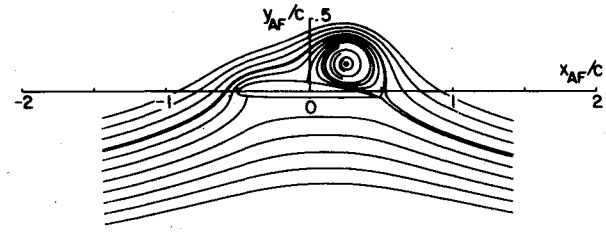

c) $x_{fl}/c = 0.50$ ($\theta_{fl} = 1.501$), $\beta_{rk} = -0.50$, $L_{fl} = 0.00$, $\Gamma_x/cU_\infty = -3.265$, $\Gamma_a/cU_\infty = 0.765$, $\dot{m}_x/cU_\infty = -0.122$, $C_L = 5.0$, $C_D = 0.25$.

Fig. 10 Streamline patterns for several flap base attachment points, $\alpha = 0.10$.

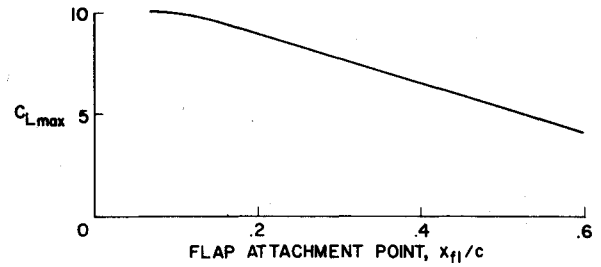

Fig. 11 Variation of maximum lift on airfoil for weak-sink solutions with chordwise location of base attachment point of flap, x_{fl}/c, $\alpha = 0.10$.

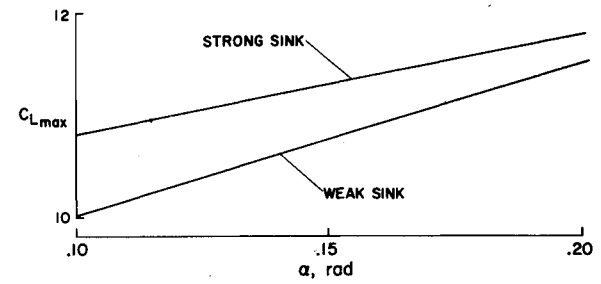

Fig. 12 Maximum lift on airfoil with externally trapped vortex as a function of airfoil angle of attack: $x_{fl}/c = 0.05$, $L_{fl} = 0.4$, $\beta_{rk} = -0.75$.

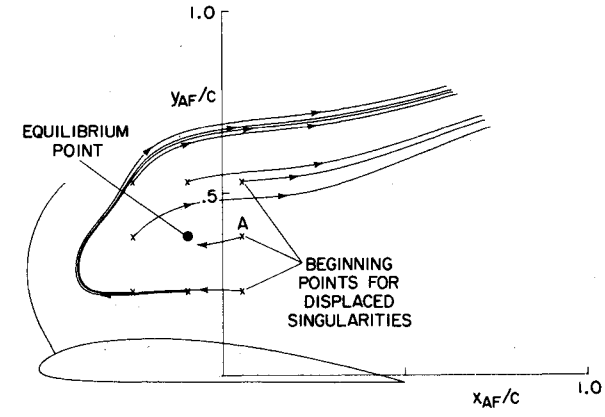

Fig. 13 Paths predicted when external singularities are displaced from equilibrium location for weak-sink case presented in Fig. 8a: $C_L = 5.08$, $C_D = 0.174$, $\Gamma_x/cU_\infty = -4.864$, $\Gamma_a/cU_\infty = 2.364$, $\dot{m}/cU_\infty = -0.0488$, $\alpha = 0.1$, $L_{fl} = 0.4$, $\beta_{rk} = -0.75$, $x_{fl}/c = 0.05$.

such as the velocity contributions of the vortex wake of the wing on the equilibrium criteria of the singularities, must be taken into account.

Since the trapped vortex is a subsonic high-lift concept, the design should be such that the magnitude of the velocity does not approach or exceed the speed of sound. One of the regions in the flowfield where this might occur is on the upper part of the vortex (where at large-lift coefficients the velocity is about 10 times the freestream velocity). Compressibility or the speed of sound will therefore serve as a limit on the lift capability of such a wing at each forward speed. Another region where compressibility effects may be a problem is at the orifice in the endplate. Since the mass flow through the orifices must not be restricted to amounts below that required to stabilize the vortex, a minimum diameter is specified for each case to keep the flow velocities subsonic.

Preliminary Experiments

Small-scale experiments that approximate the two-dimensional theoretical model were studied in the Ames 7- by 10-foot Wind Tunnel and in a 15 × 45 cm water channel. In both cases, it was possible to attain a trapped vortex behind a leading-edge flap. Since the volume capacity of the pump used at the orifice in the wind-tunnel experiment was relatively small, it was necessary to use a rear flap to further enclose and stabilize the vortex. Additionally, the inside of the cavity had to be contoured to form a smooth, circularly shaped region. Even then, the vortex existence was delicate, which agrees with the present numerical estimates of stability and with observations made in other facilities.[25-26]

The water-channel study used drain holes of various sizes in the bottom of the channel as the pumping mechanism to remove fluid from the vortex core. Trapped vortices were produced that were quite stable over a limited range of test conditions. Both the high and low sink-volume solutions were identifiable in the experiment, and a range of vortex bubble sizes with small-to-large lift coefficients could be attained. Establishment of the trapped vortex seemed to be the most difficult part of the experiment. However, once the vortex was developed, it was quite stable. Its axis, however, was not usually perpendicular to the freestream (i.e., it was not parallel to the wing or flap leading edges) but sloped at 10-20 deg to the vertical. During the starting phase, the vortex

would often precess several times before settling down to its relatively stationary, angular position. These experiments were made with the span (water depth) approximately equal to the chord of the airfoil. It is expected that external vortices will be harder to establish over larger spans.

Although these preliminary experiments were not definitive, they did show that the flowfield of the flapped airfoil with an externally trapped vortex could be established and various features of the theoretical model were confirmed qualitatively. That is, the high- and low-sink solutions and the various boundary conditions were observed to be fulfilled. Even though the flowfield appeared to have a delicate stability, they could be produced with either a single leading-edge flap or with both a leading- and a trailing-edge flap. In the water tank experiment, it was also found that the vortex flowfield was insensitive to the angle of attack of the airfoil. As already mentioned, the vortex cavity must have a smooth contour because irregularities easily disrupt the trapped vortex no matter how much suction is used.

Concluding Remarks

The present inviscid, two-dimensional analysis of the lifting characteristics of an airfoil with an externally trapped vortex indicates that lift coefficients up to around 10 are achievable. However, steady-state lift coefficients much over 10 are probably not possible with devices that are approximated by the present theoretical model, because the Kutta condition at the trailing edge of the airfoil is then violated. The major difficulty with lifting systems that use an externally trapped vortex appears to be that a steady-state external vortex is hard to generate and then maintain at its equilibrium location.

The mapping sequence used here could be extended to include a second flap located near the trailing edge of the airfoil to approximate some of the configurations tested by Kruppa[26] and others. Although some preliminary experiments have shown that such a flap helps to stabilize the external vortex, it is not certain that such an extension is the proper next step. It seems more appropriate to first consider an improved representation of the circulation distribution in the external vortex bubble. That is, in an experiment, it appears that the circulation is produced as a vortex sheet shed from the upper end of the nose flap. From there it spirals inward toward the center of the cavity and finally spanwise to an endplate orifice. A more realistic approximation to this three-dimensional distribution of vorticity and the accompanying enforcement of the Kutta condition at the trailing edges of the flap and airfoil during disturbances to the vortex position may yield stability characteristics quite different from those predicted with the point singularity model studied here.

References

[1] Prandtl, L. and Tietjens, O. G., *Applied Hydro- and Aeromechanics*, McGraw-Hill Book, Co., New York, 1934, pp. 82-85, 152-158, 282-287.

[2] "NASA Conference on V/STOL and STOL Aircraft," NASA SP-116, April 1966.

[3] "The Aerodynamics of V/STOL Aircraft," *AGARD–VKI Lecture Series*, AGARDograph 126, May 1968.

[4] Staff of NASA Langley Research Center, "VTOL and STOL Technology in Review," *Astronautics and Aeronautics*, Vol. 6, Sept. 1968, pp. 56-67.

[5] Margason, R. J., "Review of Propulsion-Induced Effects on Aerodynamics of Jet/STOL Aircraft," NASA TN D-5617, Feb. 1970.

[6] Levin, S. M., Rosen, G., and Sideris, G., "V/STOLs for the Airlines," *Space/Aeronautics*, Vol. 53, May 1970, pp. 22-47.

[7] Mavriplis, F., "Aerodynamic Research on High Lift Systems," *Canadian Aeronautics and Space Journal*, Vol. 17, May 1971, pp. 175-183.

[8] Smith, A.M.O., "High-Lift Aerodynamics," *Journal of Aircraft*, Vol. 12, June 1975, pp. 501-530.

[9] Wentz, W. H. Jr. and Kohlman, D. L., "Wind Tunnel Investigations of Vortex Breakdown on Slender Sharp-Edged Wings," NASA CR-98737, 1969.

[10] Lamar, J. E., "Recent Studies of Subsonic Vortex Lift and Parameters Affecting the Leading-Edge Vortex Stability," *Journal of Aircraft*, Vol. 14, Dec. 1977, pp. 1205-1211.

[11] Cornish, J. J. III, "High Lift Applications of Spanwise Blowing," ICAS Paper 70-09, Seventh ICAS Congress, Rome, Sept. 1970.

[12] Dixon, C. J., "Lift Augmentation by Lateral Blowing Over a Lifting Surface," AIAA Paper 69-193, AIAA and Amer. Helicopter Society VTOL Research Design and Operations Meeting, Atlanta, Ga., Feb. 1969.

[13] Dixon, C. J., Theisen, J. G., and Scruggs, R. M., "Theoretical and Experimental Investigations of Vortex-Lift Control by Spanwise Blowing," *Experimental Research*, Vol. I, Lockheed Aircraft Corp., LG73ER-0169, Sept. 1973.

[14] Bradley, R. G., Smith, C. W., and Wray, W. O., "An Experimental Investigation of Leading-Edge Vortex Augmentation by Blowing," NASA CR-132415, April 1974.

[15] Campbell, J. F., "Augmentation of Vortex Lift by Spanwise Blowing," *Journal of Aircraft*, Vol. 13, Sept. 1976, pp. 727-732.

[16] Wolff, E. B., "Preliminary Investigation of the Effect of a Rotating Cylinder in a Wing," NACA TM 307, 1925; reprinted from *De Ingenieur*, No. 49, Dec. 6, 1924, pp. 57-66.

[17] Betz, A., "The 'Magnus Effect' – The Principle of the Flettner Rotor," NACA TM 310, 1925; reprinted from *Zeitschrift des Vereines deutscher Ingenieure*, Jan., 3 1925, pp. 9-14.

[18] Ackeret, J., "Recent Experiments at Goettingen Aerodynamic Institute," NACA TM 323, 1925; reprinted from *Zeitschrift für Flugtechnik und Motorluftschiffahrt*, Feb. 14, 1925, pp. 44-52.

[19] Wolff, E. B. and Konig, C., "Tests for Determining the Effect of a Rotating Cylinder Fitted into the Leading Edge of an Airplane Wing," NACA TM 354, 1926; reprinted from Report A.105 of the *Rijks-Studiedienst Voor de Luchtvaart*, Amsterdam.

[20] Frey, K., "Experiments with Rotating Cylinders in Combination with Airfoils," NACA TM 382, 1926; reprinted from *Zeitschrift für Flugtechnik und Motorluftschiffahrt*, Aug. 28, 1926, pp. 342-345.

[21] Van der Hegge Zijnen, B. G., "Determining the Velocity Distribution in the Boundary Layer of an Airfoil Fitted with a Rotary Cylinder," NACA TM 411, 1927; reprinted from *De Ingenieur*, Oct. 23, 1926.

[22] Raspet, A., "Flight Measurements of Automatic Trailing Edge Suction on a Sailplane," Engineering Research Station, Mississippi State College, Res. Rept. No. 3, Sept. 1952.

[23] Krall, K. M. and Haight, C. H., "Wind Tunnel Tests of a Trapped Vortex-High Lift Airfoil," Advanced Technology Center, Inc., ATC Rept. No. B-94300/3TR-10, 1972.

[24] Cox, J., "The Revolutionary Kasper Wing," *Sport Aviation*, Vol. 11, July 1973, pp. 10-16.

[25] Gleason, M. and Roskam, J., "Preliminary Results of Some Experiments with a Vortex Augmented Wing," SAE Paper 720321, National Business Aircraft Meeting, Wichita, Kansas, March 1972.

[26] Kruppa, E. W., "A Wind Tunnel Investigation of the Kasper Vortex Concept," AIAA Paper 77-310, AIAA 13th Annual Meeting and Display Washington, D.C., Jan. 1977.

[27] Rossow, V. J., "Conformal Mapping for Potential Flow about Airfoils with Attached Flap," *Journal of Aircraft*, Vol. 10, Jan. 1973, pp. 60-62.

[28] "Aerodynamic Characteristics of Airfoils-IV," NACA TR 244, 1926.

[29] Theodorsen, T., "Theory of Wing Sections of Arbitrary Shape," NACA TR 411, 1932.